Chapter 2

Molecular Mechanisms of 5-Azacytidine (5AzC)-induced Toxicity in the Developing Fetal Brain

Introduction

As shown in chapter 1, 5AzC induces apoptosis and cell cycle arrest in the developing fetal brain. In the present chapter, I investigated the molecular mechanism of 5AzC-induced apoptosis and cell cycle arrest.

It is suggested that 5AzC has two effects, DNA hypomethylating effect and direct toxicity to DNA. DNA hypomethylation by 5AzC elevates expression of methylated sleeping genes, and leads the cells to differentiate (Constantinidis et al., 1977; Jones and Taylor, 1980) or to growth arrest (Bender et al., 1998). On the other hand, it is also indicated that covalent binding of DNA methyltransferase with 5AzC-containing DNA causes direct inhibition of DNA functions (DNA damage), resulting in cell cycle arrest or apoptosis (Santi et al., 1984; Michalowsky and Jones, 1987; Juttermann et al., 1994; Ferguson et al., 1997; Zhu et al., 2004; Oka et al., 2005). In the case of my experiment, it is possible that both of the mechanisms are included in the 5AzC-toxicity to the developing brain.

To find a key molecule in 5AzC-induced apoptosis and cell cycle regulation, DNA microarray analysis was carried out. From the data of microarray analysis, I first focused on the role of tumor suppressor protein p53, a trancription factor that plays a critical role in the induction of cellular growth arrest and apoptosis in response to DNA damage (May and May, 1999; Lakin and Jackson; 1999; see Fig. 2-6A). The sequential changes in the expressions of p53 and its transcriptional target genes (*$p21^{waf1/cip1}$*, *Bax*, *cyclin G1*, *Fas*, and *Gadd45*) were examined, and further p53-deficient mice were used to obtain direct evidence about the role of p53. Second, the expression

of G2/M checkpoint genes was investigated, because it was indicated from the p53-deficient experiment that G2/M arrest occurred independently of p53.

Materials and methods

All procedures were approved by the Animal Care and Use Committee of the Graduate School of Agricultural and Life Sciences, The University of Tokyo.

Animals

Jcl:Wistar rats were obtained from Japan CLEA. $p53^{+/-}$ mice were purchased from Taconic (Germantown, NY). Heterozygous mice were crossed to generate wild-type, heterozygous, and homozygous gene-disrupted mice. Endogenous and disrupted genes were detected by polymerase chain reaction analysis of tail DNA extracts, as described by Timme and Thompson (1994). Animals were kept in the same condition as shown in chapter 1.

Chemicals

5AzC was obtained from Sigma.

Experimental designs for Wistar rats

On day 13 of gestation, pregnant rats were injected i.p. with 10 mg/kg of 5AzC and then euthanized at 1, 3, 6, 9, 12, and 24 h after treatment. As controls, pregnant rats were injected with an equivalent volume of saline and euthanized at the same time

points. Collected fetuses underwent DNA microarray analysis, RT-PCR, real-time PCR, Western blotting, and immunohistochemistry.

Treatments for p53-knockout mice

Pregnant mice were injected i.p. with 10 mg/kg of 5AzC on day 12 of gestation which is corresponded to day 13 in rat, and euthanized at 6 and 12 h after treatment. As controls, dams were injected i.p. with an equivalent volume of saline on day 12 of gestation and were euthanized at 6 h after treatment. Collected fetuses were subjected to histopathological examination and cell cycle analysis.

RNA extraction and microarray analysis

Microarray analysis was performed using the Affymetrix GeneChip system (Santa Clara, CA) according to the manufacturer's instructions. Six to eight rat fetal telencephalons were acquired from each dam (6, 9, or 12 h after treatment, and controls, n = 2 dams per time point), and total RNA was extracted with the RNeasy Mini Kit (Qiagen, Germantown, MD). The quality and quantity of the extracted RNA samples were examined by agarose gel electrophoresis. Then, double-stranded cDNA was synthesized from total RNA. The first cDNA strand was prepared from 10 μg of total RNA by using SuperScript II RNase H^- Reverse Transcriptase (Invitrogen) and the T7-$(dT)_{24}$ primer (primer sequence, 5'-GGCCAGTGAATTGTAATACGACTCACTATAGGGAGGCGG-$[dT]_{24}$-3', Amersham Bioscience, Tokyo, Japan). The second strand was synthesized using the SuperScript

Double-stranded cDNA Synthesis Kit (Invitrogen). Then, biotin-labeled cRNA was synthesized from the double-stranded cDNA by using the Enzo High-yield RNA Transcription Labeling Kit (Enzo Diagnostics, NY) and purified with the RNeasy Mini Kit (Qiagen). 20 μg of biotin-labeled cRNA was then fragmented in a fragmentation buffer. Fragmented cRNA was mixed in a hybridization solution prepared with a GeneChip Eukaryotic Hybridization Control Kit (Affymetrix), and hybridized to the Affymetrix Rat Expression Array 230A for 16 h at 45°C while being rotated at 60 rpm in a GeneChip Hybridization Oven 640 (Affymetrix). The chips were then washed and stained automatically with a Fluidics Station (Affymetrix) and scanned with the GeneArray Scanner (Hewlett Packard, Palo Alto, CA).

Microarray data analysis

The microarray imaging data were analyzed using MicroarraySuite ver. 5.0 (Affymetrix). After hybridization intensity data were captured, the intensity values of each probe were calculated automatically. Data were compared between the treated and control groups. Prior to comparing any two measurements, scaling and normalizing procedures were performed. In the case of a pairwise comparison of two array results, the patterns of change of the whole probe set was used to make a qualitative call (called difference call) of "Increase (I)", "Decrease (D)", "Marginal increase (MI)", "Marginal decrease (MD)", or "No change (NC)", in which statistical analysis was done following the manufacture's guide (MicroarraySuite ver 5.0 User's Guide). The groups of genes corresponding to I, MI, D, or MD were extracted in both

samples at each time point, and cluster and pathway analyses were performed as mentioned below. The fold change in gene expression was derived from the ratio of the average difference from one experimental array compared with a control array.

The expression data (log ratio) of extracted genes and 9 other selected genes associated with cell cycle or apoptosis were subjected to hierarchical clustering analysis with Cluster 3.0 (http://rana.lbl.gov/EisenSoftware.htm), which was performed on the basis of Pearson correlation, according to the theory and methods provided in the manual. The assembled clustering data were visualized with TreeView (http://rana.lbl.gov/EisenSoftware.htm).

The extracted genes also underwent signal pathway analysis with GenMAPP (http://www.GenMAPP.org). This analysis involves the uploading of gene expression data onto known biologic pathways and a list of genes that is categorized with gene functions. Data regarding each gene are easily visualized, including its change in expression and roles in various signal cascades.

Real-time PCR and PCR

Total RNA was reverse-transcribed for first-strand cDNA synthesis with an oligo $(dT)_{12-18}$ primer and SuperScript II RNase H^- Reverse Transcriptase (Invitrogen). Real-time PCR was performed using oligonucleotide primers sets corresponding to the cDNA sequences of *cyclin B1*, *Cdc20*, and *glyceraldehyde-3-phosphate dehydrogenase (Gapdh).* Sense and antisense primers were as follows: *cyclin B1*, 5'-CAGAGGTGGAACTGGATGAGC-3' and 5'- GGGCTTGGAGAGGGAGTATCA-3',

respectively; *Cdc20*, 5'- AGGAGGTACCAGTGACCGACA-3' and 5'-ACCAGAGGATGGAGCACACC-3', respectively; and *Gapdh*, 5'-CCTGCACCACCAACTGCTTAG-3' and 5'- CATGGACTGTGGTCATGAGCC-3', respectively. In brief, 25 μl of reaction mixture containing 12.5 μl SYBR Green Real-time PCR Master Mix (Toyobo, Osaka, Japan), 0.2 μM each of the sense and antisense primers, and 1 μl of the cDNA sample was preheated at 95°C for 3 min and then underwent 40 cycles of amplification (denaturation at 95°C for 15 sec, annealing and extension at 60°C for 1 min) by using the ABI PRISM 7900HT Sequence Detection System (Applied Biosystems, Foster City, CA). Relative intensity against *GAPDH* was calculated, and fold change relative to the control was represented as the mean ± SD of 2 dams.

PCR was performed using oligonucleotide primer sets corresponding to the cDNA sequences of *p53*, p53-target genes (*p21* $^{waf1/cip1}$, *Bax*, *cyclin G1*, *Fas*, and *Gadd45*) and *Gapdh*. Sense and antisense primers were as follows: *p53*, 5'-ATATGAGCATCGAGCTCCCTCT-3' and 5'-CACAACTGCACAGGGCATGT-3', respectively (23 cycles); *p21* $^{waf1/cip1}$, 5'-AAGTATGCCGTCGTCTGTTCG-3' and 5'-GGCACTTCAGGGCTTTCTCTT-3', respectively (31 cycles); *Bax*, 5'-TTCATCCAGGATCGAGCAGAG-3' and 5'-TGAGGACTCCAGCCACAAAGAT-3', respectively (25 cycles); *cyclin G1*, 5'-GTGTCGGACTGAGCTGCTTTT-3' and 5'-TTGGGAGGTGGGTTATCCTGT-3', respectively (23 cycles); *Fas*, 5'-AAGAGGAGCGTTCGTGAAACC-3' and 5'-GATCAGCAGCCAAAGGAGCTTA-3', respectively (29 cycles); *Gadd45*, 5'-GATCGAAAGGATGGACACGG-3' and 5'-

CCCACTGATCCATGTAGCGA-3′, respectively (27 cycles); and *Gapdh*, 5′-GAGTAT-GTCGTGGAGTCTACTG-3′ and 5′- GCTTCACCACCTTCTTGATGTC-3′ (21 cycles). In brief, 100 μl of reaction mixture containing 10 μl 10× PCR buffer (100 mM Tris·HCl buffer, 500 mM KCl, and 15 mM $MgCl_2$; Takara, Shiga, Japan), 10 μl dNTP (Takara), 50 pmol each of sense and antisense primers, and 1 μl of the cDNA sample, was pre-heated at 95 °C for 5 min, and a PCR reaction cycle (× each cycle number) of denaturation at 95 °C for 1 min, annealing at 58 °C for 1 min, and extension at 72 °C for 1 min was performed in a Takara PCR Thermal cycler SP (Takara). The PCR products were electrophoresed and stained with ethidium bromide. Fluorescent bands were visualized using a UV-CCD video system (EpiLight $_{UVFA1100}$; AISIN COSMOS, Tokyo, Japan) and were analyzed using an image-analysis software, Quantity One (pdi, NY). Relative intensity of the band against *Gapdh* band was represented as the mean ± SD of 5 dams. Statistical analysis was carried out by Student's *t*-test, Mann-Whitney's U test, or Weltch's *t*-test.

Western blotting

Four or five rat fetal telencephalons (3 to 12 h after treatment, and controls) were homogenized in a solution of 20 mM Tris-HCl (pH 7.4) containing 150 mM NaCl, 1 mM PMSF, 1% aprotinin, 2 mM EDTA, 2 mM Na_3VO_4, 1% NP-40, 0.1% SDS and 1 mM DTT, and centrifuged at 12000 g for 20 min at 4°C. Approximately 30 μg of extract was loaded per lane of a 10% SDS–PAGE gel, electrophoresed, and transferred to a PVDF membrane (Bio-Rad, Hercules, CA). Blots were first probed with

antibodies to p53 (Santa Cruz, Santa Cruz, CA), Chk2 (Santa Cruz), $p21^{waf1/cip1}$ (Pharmingen), cyclin B1 (NeoMarkers, Fremont, CA), Cdc2 (Cell Signaling Technology), phospho-Cdc2 (Tyr16) (Cell Signaling Technology), and β-actin (Sigma). After incubation with the appropriate secondary antibody conjugated to horseradish peroxidase (Amersham, Buckinghamshire, UK), detection was performed with the ECL Plus kit (Amersham).

TUNEL method

Cells with DNA fragmentation (apoptotic cells) were detected by the TUNEL method as described in chapter 1.

Immunohistochemistry

Collected fetuses were fixed in 10% neutral-buffered formalin and embedded in paraffin. The dorsal telencephalic wall was mainly examined. Three antibodies for p53-related proteins were used for immunohistochemical staining; rabbit anti-p53 polyclonal antibody (1:300; Santa Cruz), mouse anti-$p21^{waf1/cip1}$ monoclonal antibody (1:100; PharMingen), and rabbit anti-Bax polyclonal antibody (1:300; Santa Cruz) with Envision+ Kit (Dako). Paraffin sections (thickness, 4 μm) were immersed in 10 mM citrate buffer, pH 6.0, and heated for 15 min at 120 °C by autoclave. Immunohistochemical staining for cleaved caspase-3 and phospho-histone H3 were undertook as described in chapter 1. The signals were visualized by peroxidase-DAB reaction and then counterstained with methyl green.

Cell cycle analysis

The telencephalons of fetuses from each dam were obtained carefully under stereoscopic microscopy. They were then prepared for flow cytometric analysis using propidium iodide (PI; 50 μg/ml, Sigma) staining as described in chapter 1.

Results

As described in chapter 1, apoptosis with similar nature occurred in all fetal brain regions, i.e. telencephalon, diencephalon, mesencephalon and metencephalon, following 5AzC-treatment to dams on gestation day 13 (Fig. 1-2B). Therefore, the telencephalon was mainly observed in this study.

DNA microarray analysis

DNA microarray analysis was undertaken to seek the key factors in apoptosis, the cell-cycle arrest and other cellular responses to 5AzC. According to the criteria described in Materials and Methods, 249 increased and decreased genes were extracted (Table 2-1), and further 9 genes (*Cdk4*, *Cdk5*, *cyclin D1*, *cyclin E1*, *p27*, *Pcna*, *Cdc25b*, *caspase 8*, and *Bax*) associated with cell cycle regulation or apoptosis were selected. In the cluster analysis, specific expression patterns were observed at each time point (Fig. 2-1). The genes were roughly divided into 5 clusters (A to E) for categorizing them by expression pattern. The expression of some target genes of p53 ($p21^{waf1/cip1}$, *cyclin G1*, *Igfbp3*, *Mdm2*, *Snk*) was upregulated from 6 to 12 h (Table 2-1). In

addition, the expression of some genes involved in the cell cycle regulation was also changed from 6 to 12 h; most of them were included in cluster D. Expression of two genes regulating the G2/M transition, *cyclin B1* and *Cdc20*, was enhanced mainly at 12 h (Table 2-1 and Fig. 2-5B).

In addition to the cell-cycle-regulating genes, other genes also showed characteristic changes in expression (Table 2-1). The expression of chaperones, proteins that fold and modify other proteins in the endoplasmic reticulum, decreased through the 6- and 12-h time points, and the expression patterns of chaperones were similar to each other and belonged to cluster B (Table 2-1). Similarly, the expression of cholesterol synthesis genes also decreased at 6 through 12 h and showed a cluster B-type pattern. In contrast, genes involved in amino acid metabolism were allocated into cluster E on the basis of their expression, which increased mainly at 6 to 9 h. The expression of growth factors categorized into cluster D was upregulated at 12 h. What these changes in expression indicate is unclear yet, but 5AzC-treatment may exert unknown effects on neural progenitor cells.

Expression of p53 and its target genes

In chapter 1, it was demonstrated that 5AzC induces apoptosis and G2/M arrest. Because 5AzC is a DNA demethylating and damaging agent (Fig. I-3B), I focused on the role of p53, a transcription factor that plays an important role in apoptosis and cell cycle arrest induced by DNA damage.

First, PCR was undergone to detect the expression of p53 and its target genes

mRNAs. The results of PCR are shown in Fig. 2-2A and B. As compared to controls, the expression levels of *p21* $^{waf1/cip1}$ and *cyclin G1* mRNAs were significantly elevated from 9 to 24 h, that of *Bax* mRNA at 12 h, and that of *Fas* mRNA from 9 to 12 h, respectively. On the other hand, there was no significant elevation in the expression levels of *p53* and *Gadd45* mRNAs.

In Western blotting, the expression of p53 protein was elevated during 6 h through 12 h (Fig. 2-2C). The expression of $p21^{waf1/cip1}$, a CDK inhibitor and target gene of p53, also increased (Fig. 2-2C).

Immunohistochemically, TUNEL-, p53-, $p21^{waf1/cip1}$- and Bax-positive cells were observed in the telencephalic wall. To compare the localization of each positive cell, the telencephalic wall was divided into 5 areas (DF, outer area, middle area, inner area, and mitotic cells) as done in migration study in chapter 1 (Fig. I-2B, 1-6).

TUNEL-positive apoptotic cells appeared at 9 h in the VZ, mainly in the inner and middle areas (Fig. 1-2A-c, 2-3B). The number of apoptotic cells peaked at 12 h, and slightly decreased at 24 h (Fig. 1-2C and 2-3B). Apoptotic cells were observed mainly in the middle area at 12 h, and both in the outer area and the DF at 24 h (Fig. 2-3B).

Few p53-positive cells were observed in the telencephalic wall of control fetuses (Fig. 2-3A-a). In the telencephalic wall of 5AzC-treated fetuses, p53-positive cells appeared at 6 h in the inner and middle areas (Fig. 2-3A-b). The number peaked at 9 h, and decreased gradually from 12 to 24 h (Fig. 2-3A, B). p53-positive cells were observed mainly in the inner area at 9 h, and in the middle area at 12 h (Fig. 2-3A-c, d, B). p53 seemed to be expressed prior to the development of apoptosis, and their

localization was similar to apoptotic cells which appeared in the inner and middle areas. This suggests that apoptosis is induced by p53 dependent mechanism.

The localization of $p21^{waf1/cip1}$-positive cells well corresponded to that of p53-positive cells. A few $p21^{waf1/cip1}$-positive cells were observed in a part of DF of the control telencephalic wall (Fig. 2-3A-e). $p21^{waf1/cip1}$-positive cells appeared at 6 h mainly in the inner area, and the number increased in the middle area at 9 h (Fig. 2-3A-f, g, B). The number peaked at 12 h, when $p21^{waf1/cip1}$-positive cells were localized mainly in the middle and outer areas (Fig. 2-3A-h, B).

Few Bax-positive cells were seen in the control telencephalic wall (Fig. 2-3A-i). Bax-positive signals were observed in some pyknotic cells from 12 to 24 h (Fig. 2-3A-j, k). They were seen more prominently in the regions in which apoptotic cells accumulated.

The role of p53

The results of expression patterns of p53 and its target genes indicate that p53 is involved in 5AzC-induced toxicity. Cell cycle alteration in p53-knockout mice was therefore examined to confirm the influence of p53 on the cell cycle and apoptosis. 5AzC-induced pathological changes, apoptosis and cell cycle arrest, looked like similar between rat and mouse (wild-type) fetuses (Fig. 2-4). Histopathological evaluation revealed abnormal accumulation of mitotic cells along the ventricle at 6 h in every p53 genotype (Fig. 2-4A-a–c). These mitotic cells were positive for phospho-histone H3 (Fig. 2-4A-g–i). At 12 h, pyknotic cells positive for cleaved caspase-3 were observed

in the $p53^{+/+}$ (wild-type) and $p53^{+/-}$ mice, but not in the $p53^{-/-}$ mice (Fig. 2-4A-d–f, j–l). p53- and $p21^{waf1/cip1}$-positive cells appeared only in wild-type and $p53^{+/-}$ mice (Fig. 2-4A-m–r), indicating that the expression of $p21^{waf1/cip1}$ depends on p53. In the cell cycle analysis (Fig. 2-4B), G2/M arrest was observed in every phenotype at 6 h (+/+, 15.7 ± 1.0%; +/–, 14.4 ± 1.9%; –/–, 14.2 ± 0.7%), but at 12 h, the number of apoptotic cells in the sub-G1 area increased only in the $p53^{+/+}$ and $p53^{+/-}$ mice (+/+, 21.2 ± 6.3%; +/–: 11.2 ± 3.1%; –/–, 2.8 ± 1.5%). $p53^{-/-}$ neural progenitor cells escaped from apoptosis at 12 h, although the number of cells in the G2/M phase increased through the 6- and 12-h time points. These results suggest that 5AzC-induced apoptosis is p53-dependent and that the associated G2/M arrest is p53-independent. At 12 h, the number of mitotic cells decreased in every p53 genotype, suggesting that G2 arrest occurs in the $p53^{-/-}$ fetal brain. Although S phase arrest also occurred at 6 to 12 h in the $p53^{+/+}$ animals, it occurred only at 6 h in the $p53^{-/-}$ mice. Therefore p53 may play a role in maintaining the S phase arrest.

G2/M checkpoint

In the pathway analysis on the data of DNA microarray, I noted enhanced expression (mainly at 12 h) of two genes regulating the G2/M transition (*cyclin B1* and *Cdc20*) (Fig. 2-5A). The increased expression of these genes mRNAs was confirmed by using real-time PCR (Fig. 2-5B). In light of the results in the $p53^{-/-}$ fetal brain, I focused on the p53-independent cascade regulating G2/M transition. Western blotting was used to examine the expression of proteins which regulate G2/M transition, cyclin

B1, Cdc2 (Cdk1), phospho-Cdc2 (Tyr16), and Chk2 protein (Fig. 2-5C, 2-6B). Expression of cyclin B1 increased from 3 to 9 h. The amount of phosphorylated Cdc2, an inactivated form of Cdc2, was lowest at 6 h and gradually increased from 9 to 12 h, whereas the expression of Cdc2 was nearly unchanged throughout the experimental period. The expression and mobility of Chk2 protein did not change through the experimental period.

Discussion

In this chapter, I showed that 5AzC-triggered apoptosis is induced by a p53-dependent mechanism, and G2/M arrest probably occurs in a p53-independent manner. The molecular mechanism of 5AzC-induced toxicity in the developing fetal brain is summarized in Fig. 2-6C, which is combined with the results in chapter 1.

DNA damage and the role of p53

p53 protein is known as a "guardian of genome", and plays a critical role in DNA repair, cell cycle arrest, and apoptosis in response to DNA damage (Fig. 2-6A; Lakin and Jackson, 1999). In the CNS of fetuses, p53 expression increased in response to DNA damage, e.g. radiation (Bolaris et al., 2001) or ENU administration (Katayama et al., 2002), and this indicates that fetal neuroepithelial cells have potential to respond to DNA damage mediated by p53. In the present study, p53-positive cells appeared at 6 h, and their number peaked at 9 h, prior to the development of apoptosis, suggesting that p53 protein respond to 5AzC-induced toxicity to DNA. Indeed, I showed that

apoptosis was induced in a p53-dependent manner because apoptosis was not induced in $p53^{-/-}$ fetal brain (Fig. 2-4). It is reported that 5AzC or 5-aza-2'-deoxycytidine, which has deoxyribose instead of ribose in 5AzC, is incorporated into DNA, and forms covalent bond with DNA methyltransferase (Santi et al., 1984; Michalowsky and Joned, 1987; Ferguson et al., 1997), resulting in DNA damage (Juttermann et al., 1994; Karpf et al., 2001; Zhu et al., 2004; Oka et al., 2005). It is supposed that these mechanisms are also involved in the present experimental model. It is further suggested that p53 protein induction after 5AzC administration does not result from hypomethylated re-expression, because p53 mRNA did not increase after 5AzC administration. The activity of p53 is known to be regulated by Mdm2 protein in a post-translational mechanism (Lakin and Jackson, 1999). Such a mechanism may, therefore, regulate p53 protein expression in this study.

p53 protein activates the transcription of various genes in response to DNA damage (May and May, 1999; Fig. 2-6A). In this study, five p53-transcriptional target genes, *$p21^{waf1/cip1}$* (el-Deiry et al., 1993), *Bax* (Selvakumaran et al., 1994), *cyclin G1* (Okamoto and Beach, 1994), *Fas* (Muller et al., 1998), and *Gadd45* (Kastan et al., 1992) were investigated. $p21^{waf1/cip1}$ is an inhibitor of cyclin-dependent kinases and it induces cell cycle arrest at G1 or G2 phase (Dulic et al., 1994). Bax is a pro-apoptotic member of bcl-2 family. Increased Bax/Bcl-2 ratio enforces dimerization of Bax, and finally induces apoptosis (Gross et al., 1998). Cyclin G1 is included in a negative feedback loop, where it activates Mdm2 to degrade p53 protein (Okamoto et al., 2002; Ohtsuka et al., 2004). Fas is a type I membrane protein which belongs to tumor necrosis factor

receptor / nerve growth factor receptor family (Itoh et al., 1991), and it induces apoptosis when it binds to Fas ligand (Nagata and Golstein, 1995). Gadd45 is reported to play an important role in DNA repair (Smith, 1994). In this study, Bax and Fas, which are apoptosis-related proteins, may act as an apoptosis-inducer, because their mRNA levels were elevated and Bax protein was seen in apoptotic cells. The expression of *Bax*, *Fas*, and *cyclin G1* mRNAs was elevated following p53 protein expression, from 9 to 24 h (Fig. 2-2). p53 may, therefore, transactivate these genes. $p21^{waf1/cip1}$ increased both in mRNA and protein levels following the elevation of p53 protein expression, and the region of $p21^{waf1/cip1}$-expressing cells was similar to that of p53-positive cells (Fig. 2-2, 2-3). Additionally in p53-deficient mice, $p21^{waf1/cip1}$ expression was diminished (Fig. 2-4A-r), indicating that $p21^{waf1/cip1}$ was expressed through a p53-dependent pathway. The function of $p21^{waf1/cip1}$ protein is to induce G1/S or G2/M arrest as mentioned above. In the present study, G2/M arrest is independent of p53 cascade. $p21^{waf1/cip1}$ therefore may play a role in G1 phase after mitosis where most of apoptotic cell death occurred in this experiment (Fig. 1-7).

DNA demethylating effect of 5AzC

5AzC also can disturb gene expression and alter organogenesis through its DNA demethylating effect. Although DNA microarray analysis was performed, it failed to identify any gene whose expression was upregulated by the demethylating effect. However, only a few genes currently are known to be transcriptionally regulated by DNA methylation in the developing brain. For example, the astroglial markers GFAP

and S100β are hypermethylated in the early to mid developing brain before glial cells are produced (Takizawa et al., 2001; Sun et al., 2003; Namihira et al., 2004; Fan et al., 2005), however their expression was unchanged at 6 to 12 h after 5AzC treatment (data not shown). Therefore, it was difficult to definitively determine the role of 5AzC-induced demethylation in neural progenitor cells of the developing brain. It is supposed that the effect of 5AzC shows a dose dependency, because 5AzC induces cell differentiation via DNA hypomethylation at low doses (Jones and Taylor, 1980) and DNA damage at high doses (Michalowsky and Jones, 1987; Egger et al., 2004). The dose used in this study is a high dose that may prefer the covalent attachment of DNA methyltransferases and 5AzC-containing DNA, which leads to DNA damage. In some contexts, however, disturbance of the methylation state of the DNA from its normal pattern such as loss of DNA methyltransferase causes elevated p53 expression and cell death (Jackson-Grusby et al., 2001; Dodge et al., 2005). Therefore, it is difficult to exclude the possibility that the toxicity of 5AzC is associated with a DNA demethylating effect.

G2/M checkpoint

I have shown that 5AzC induces a p53-dependent apoptosis (Fig. 2-4). In contrast, the 5AzC-associated G2/M arrest seems to be p53-independent. In the microarray and signal pathway analyses, the expression of genes that promote G2/M transition (*cyclin B1* and *Cdc20*) was upregulated (Fig. 2-5A, B), so an alternative pathway of cell cycle regulation was investigated. For the G2 to M transition, the activation of Cdc2 kinase

(Cdk1) and its interaction with cyclin B1 are indispensable (Fig. 2-6B). Chk1 and Chk2 are serine kinases, which are activated in response to DNA damage (Chaturvedi et al., 1999; Liu et al., 2000; Matsuoka et al., 2000) and lead to G2 arrest through inactivation of Cdc2. The Cdc2–cyclin B complex becomes inactive after phosphorylation of tyrosine 15 and threonine 14 of Cdc2. Cdc25 dephosphorylates and activates Cdc2, but Chk1 and Chk2 phosphorylate and sequester Cdc25 in the cytoplasm, where it is ineffective. As a result, Cdc2 becomes phosphorylated and inactive. In some G2 arrest models, the arrest is reported to be brought about by Chk1 or Chk2, independent of p53 (Taylor and Stark, 2001; Iliakis et al., 2003).

However, in the present study, phospho-Cdc2 decreased although G2 arrest occurred (Fig. 2-5C). This abnormal activation of Cdc2 might accelerate the G2 to M transition, probably resulting in accumulation of mitotic cells. Further, the expression of cyclin B1 was slightly increased at 3 to 9 h (Fig. 2-5C). Cyclin B1 is degraded by anaphase-promoting complex (APC) at metaphase, and this process is indispensable for mitotic progression, so the accumulation of cyclin B1 observed might occur as a result of inactivation of APC, which leads to mitotic arrest (Nitta et al., 2004). The mitotic cells observed in chapter 1 have abnormal morphologies, such as dispersed chromatin and intact nuclear membranes (Fig. 1-1C). Recently, mitotic catastrophe, a type of cell death occurring during or after mitosis with some mitotic failure, has been proposed (Castedo et al., 2004). Although the definition of this cell death yet differs among researchers, 5AzC-induced abnormal mitosis and subsequent apoptosis might fall into this category. Indeed, aberrant entry into mitosis after DNA damage, gene deficiencies,

or excess activation of Cdc2–cyclin B1 each suffice to cause mitotic catastrophe (Castedo et al., 2004; Niida et al., 2005), which is consistent with the present model that includes DNA damage and Cdc2 activation. In addition, Serum-inducible kinase (Snk/Plk2), which is induced by p53, likely is an inhibitor of mitotic catastrophe (Burns et al., 2003). In the microarray study, upregulated expression of *Snk/Plk2* was detected at 9 h, when abnormal mitosis began to decrease (Table 2-1). This result also supports the idea that mitotic catastrophe occurred. Further investigation is needed to clarify whether these mitotic cells with abnormal morphology produce two daughter cells with diploid DNA or generate tetraploid G1 cells by mitotic failure; although the results from the BrdU incorporation assay suggest that some of the cells can produce diploid cells (Fig. 1-5). Regardless, at 9 to 12 h, the amount of activated Cdc2 increased compared with that at 6 h (Fig. 2-5C), and the number of mitotic cells gradually decreased (Fig. 1-1A, B). This pattern suggests that abnormal mitotic entry is suppressed and normal G2 arrest is induced, although the expression level and phosphorylation state of Chk2, the regulator of the G2 checkpoint after DNA damage, did not change (Fig. 2-5C). The mechanism of the G2 arrest is still obscure, but from the study in p53-deficient mice, a p53-independent mechanism may be involved.

Many environmental stresses have a potential to disturb the processes of brain development, i.e. proliferation, migration, and differentiation of neural cells, however their mechanisms remain unclear (Rodier, 1995; Mendola et al., 2000; Costa et al., 2004). The present study revealed how neural cells in the developing brain respond to

extrinsic stimuli regarding with the molecular mechanisms of proliferation and cell death, which will offer important information to the mechanisms of fetal brain toxicity induced by widespread environmental stresses.

Summary

5AzC induces apoptosis and G2/M arrest in the developing fetal brain. In this chapter, the molecular mechanisms that induce apoptosis and cell cycle arrest were examined. First, DNA microarray analysis was undertaken, and elevated expression of target genes of tumor suppressor gene p53, which plays a critical role in response to DNA damage, was detected. Expressions of p53 protein and its target gene mRNAs and proteins increased and were expressed in the VZ prior to the appearance of apoptotic cells. In 5AzC-treated p53-deficient fetal brains, apoptosis did not occur, although G2/M arrest was induced. These results suggest that in the developing brain, apoptosis is p53-dependent, but that another mechanism governs the G2/M checkpoint. The G2/M regulator, Cdc2, was activated by dephosphorylation through G2/M accumulation, suggesting accelerated entry into mitosis leading to accumulation of cells showing abnormal mitosis. The present results revealed that the neural progenitor cells use several molecular mechanisms to regulate cell death and cell cycle progression toward the extrinsic stresses.

Accession No.	Genes	Fold change 6h	9h	12h	Cluster
Cell cycle					
NM_022183.1	topoisomerase II alpha (Top2a)		1.3±0.09		E
U05341.1	Cdc20 / p55CDC			1.52±0.09	D
X64589.1	cyclin B (Ccnb1)			1.40±0.16	D
NM_012760.1	lost on transformation 1 (Lot1) / pleiomorphic adenoma gene-like 1 (Plagl1) / Zac1	-1.17±0.05			D
NM_054008.1	rgc32 protein (Rgc32)			-1.98±0.47	A
NM_022683.1	vasopressin-activated calcium-mobilizing receptor protein (VACM-1) / cullin-5 (Cul5)			-1.77±0.72	A
NM_021662.1	DNA polymerase delta, catalytic subunit (Pold1)			-1.52±0.17	A
NM_017258.1	B-cell translocation gene 1, anti-proliferative (Btg1)			-1.37±0.20	A
p53-target genes					
NM_012923.1	cyclin G1 (Ccng1)	1.93±0.00	3.02±0.38	3.23±0.03	D
U24174.1	p21 (Waf1 / Cip1)		4.10±2.77		E
BF548539	ESTs, Moderately similar to mouse mdm2 protein		1.63±0.04		D
NM_031821.1	serum-inducible kinase (Snk) / Plk2		1.42±0.19		D
NM_012588.1	insulin-like growth factor-binding protein (Igfbp3)		2.30±0.98	1.86±0.32	D
Growth factor					
NM_022266.1	connective tissue growth factor (Ctgf)			1.55±0.01	D
NM_019198.1	fibroblast growth factor 17 (Fgf17)			1.52±0.24	D
NM_030859.1	midkine (Mdk)			1.26±0.04	D
Chaperone					
M14050.1	heat shock 70kD protein 5 (Hspa5) / Immunoglobulin heavy chain binding protein (Bip) / Grp78	-1.62±0.21	-2.04±0.10		B
NM_022399.1	calreticulin (Calr)	-1.45±0.25	-1.65±0.17		B
AI412322	t-complex 1 (Tcp1) / chaperonin-containing t-complex polypeptide 1 (Cct)	-1.40±0.03	-1.32±0.05		B
BI284965	calcium binding protein 1 (Cabp1)		-1.36±0.07		B
NM_053849.1	protein disulfide isomerase related protein (Erp70)		-1.68±0.20	-1.77±0.21	B
NM_017319.1	ER-60 protease (ER60) / glucose regulated protein, 58 kDa (Grp58) / oxidoreductase ERp57			-1.51±0.21	B
Cholesterol synthesis					
NM_022389.1	7-dehydrocholesterol reductase (Dhcr7)	-1.47±0.11			B
NM_017136.1	squalene epoxidase (Sqle)	-1.42±0.13			B
NM_019238.1	farnesyl diphosphate farnesyl transferase 1 (Fdft1) / squalene synthase	-1.40±0.08	-1.35±0.05		B
NM_080886.1	sterol-C4-methyl oxidase-like (Sc4mol) / neurorep 1	-1.34±0.22	-1.50±0.22		B

Accession No.	Genes	Fold change 6h	9h	12h	Cluster
NM_013134.1	3-hydroxy-3-methylglutaryl-Coenzyme A reductase (Hmgcr)		-1.52±0.12		B
NM_022392.1	growth response protein (CL-6) / Insig1	-1.65±0.11	-2.41±0.79	-1.57±0.12	B
NM_017268.1	3-hydroxy-3-methylglutaryl-Coenzyme A synthase 1 (Hmgcs1)	-1.45±0.08	-1.60±0.22	-1.66±0.12	B
NM_031840.1	farnesyl diphosphate synthase (Fdps) / dimethylallyltransferase / geranyl-trans transferase	-1.42±0.15	-1.76±0.14	-1.75±0.10	B
NM_053539.1	isopentenyl-diphosphate delta isomerase (Idi1)	-1.33±0.12	-1.71±0.26	-1.64±0.08	B
Amino acid metabolize					
NM_024403.1	activating transcription factor ATF-4 (Atf4)	1.85±0.52			E
NM_013111.1	solute carrier family 7 member A1 (amino acid transporter cationic 1) (Slc7a1)	1.81±0.52			E
NM_017353.1	tumor-associated protein 1 (TA1) / Slc7a5	2.84±0.55	1.76±0.04		E
NM_019283.1	solute carrier family 3 (activators of dibasic and neutral amino acid transport), member 2 (Slc3a2)	1.86±0.47	1.59±0.12		E
U07202.1	asparagine synthetase (Asns)	3.09±1.61	3.06±1.14	2.69±0.19	D
Cytoskeleton					
BG378086	Map1b / microtubule-associated protein 5 (Map5)	-1.37±0.09			B
AA946388	myosin heavy chain 11	-1.33±0.03			B
NM_012987.1	nestin (Nes)		-1.34±0.04		B
Nuclear membrane					
AI407364	lamin B1 (Lmnb1)	-1.26±0.08			C
Others					
NM_080906.1	HIF-1 responsive RTP801 (Rtp801)	1.49±0.12	1.59±0.09		E
NM_012578.1	histone H1-0 (H1f0)	1.31±0.04	1.42±0.06		E
BM383531	metallothionein 2 (Mt1) and metallothionein 1 (Mt2)	1.85±0.05	1.55±0.54	2.55±0.83	D
U65656.1	gelatinase A (GelA) / matrix metalloproteinase 2 (Mmp2)		1.41±0.09		D
NM_013087.1	CD81 antigen (target of antiproliferative antibody 1)		1.29±0.02		D
AF154349.1	legumain (Lgmn) / asparaginyl endopeptidase (Aep)			1.56±0.25	D
NM_134351.1	methionine adenosyltransferase II, alpha (Mat2a)			1.39±0.05	D
BF417032	transferrin receptor (Tfrc)			1.37±0.15	D
NM_012681.1	transthyretin (prealbumin, amyloidosis type I) (Ttr)			1.32±0.17	D
NM_057100.1	growth arrest specific 6 (Gas6)	-1.27±0.07			B
BM386513	clathrin, heavy polypeptide (Hc) (Cltc)	-1.22±0.18			C
NM_013219.1	Ca2+-dependent activator protein (Caps)	-1.37±0.09	-1.39±0.03		B
BF417262	hepatocarcinogenesis-related transcription factor (Htf)	-1.34±0.15	-1.42±0.02		B
NM_022546.1	death-associated like kinase (Dapkl)		-1.96±0.54		

Accession No.	Genes	Fold change 6h	9h	12h	Cluster
M55292.1	neural receptor protein-tyrosine kinase (TrkB)			-1.82±0.05	B
NM_012889.1	vascular cell adhesion molecule 1 (Vcam1)			-1.60±0.06	A
NM_031564.1	Eph receptor A3 (Epha3)			-1.61±0.24	A
NM_013190.1	phosphofructokinase, liver, B-type (Pfkl)			-1.49±0.16	A
NM_012733.1	retinol-binding protein 1 (Rbp1) / Crbp1			-1.48±0.10	A
NM_033235.1	malate dehydrogenase-like enzyme (Mdhl)			-1.43±0.25	A

Table 1. Gene expression changes in the rat fetal telencephalon treated with 5AzC. Fold change is presented as the mean ± SD of 2 arrays.

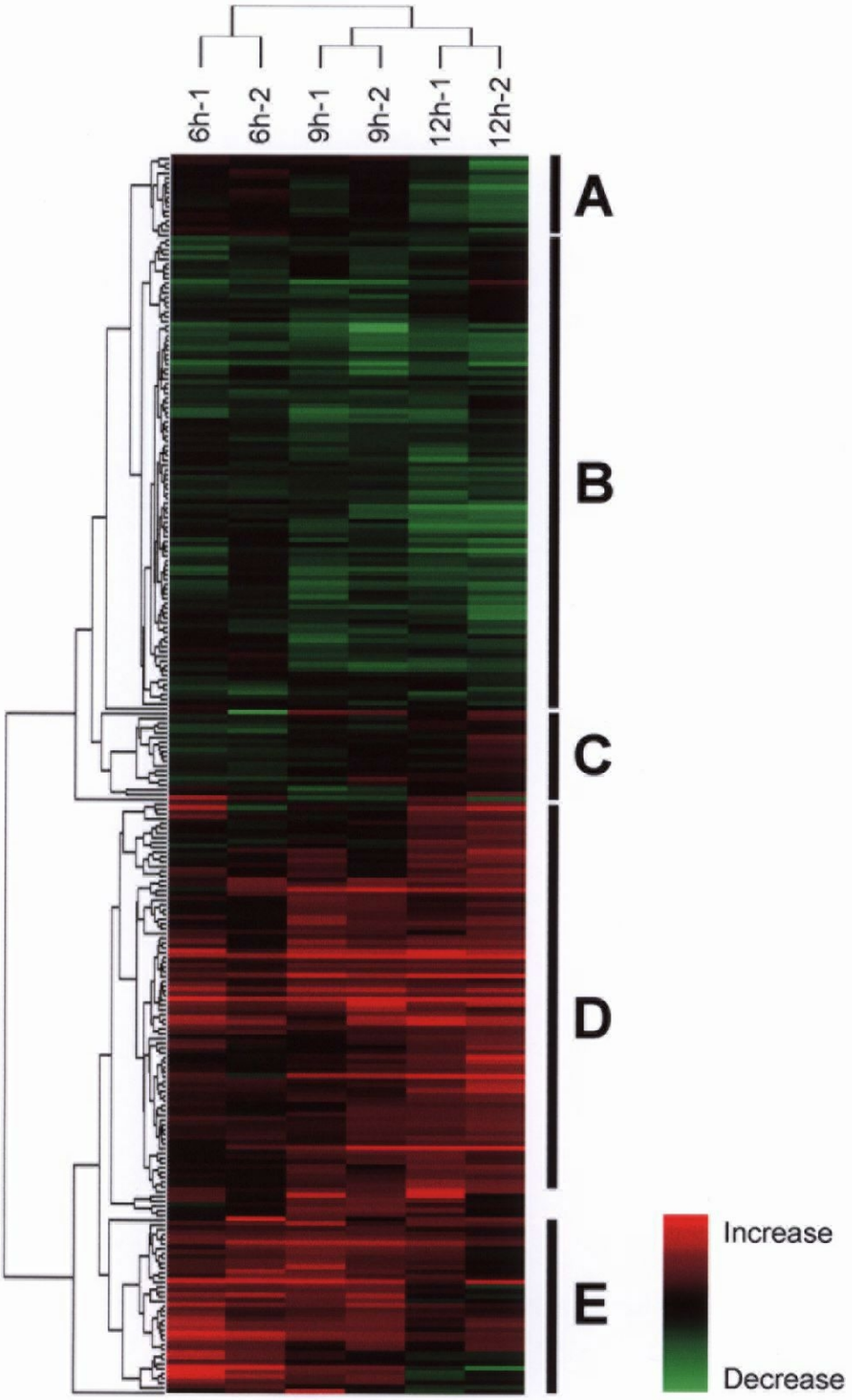

Fig. 2-1. Cluster analysis of up (red) and downregulated (green) genes in DNA microarray analysis. I divided the genes into 5 clusters (A to E) according to the expression patterns. The genes have characteristic expression patterns in each time point (6, 9, and 12 h).

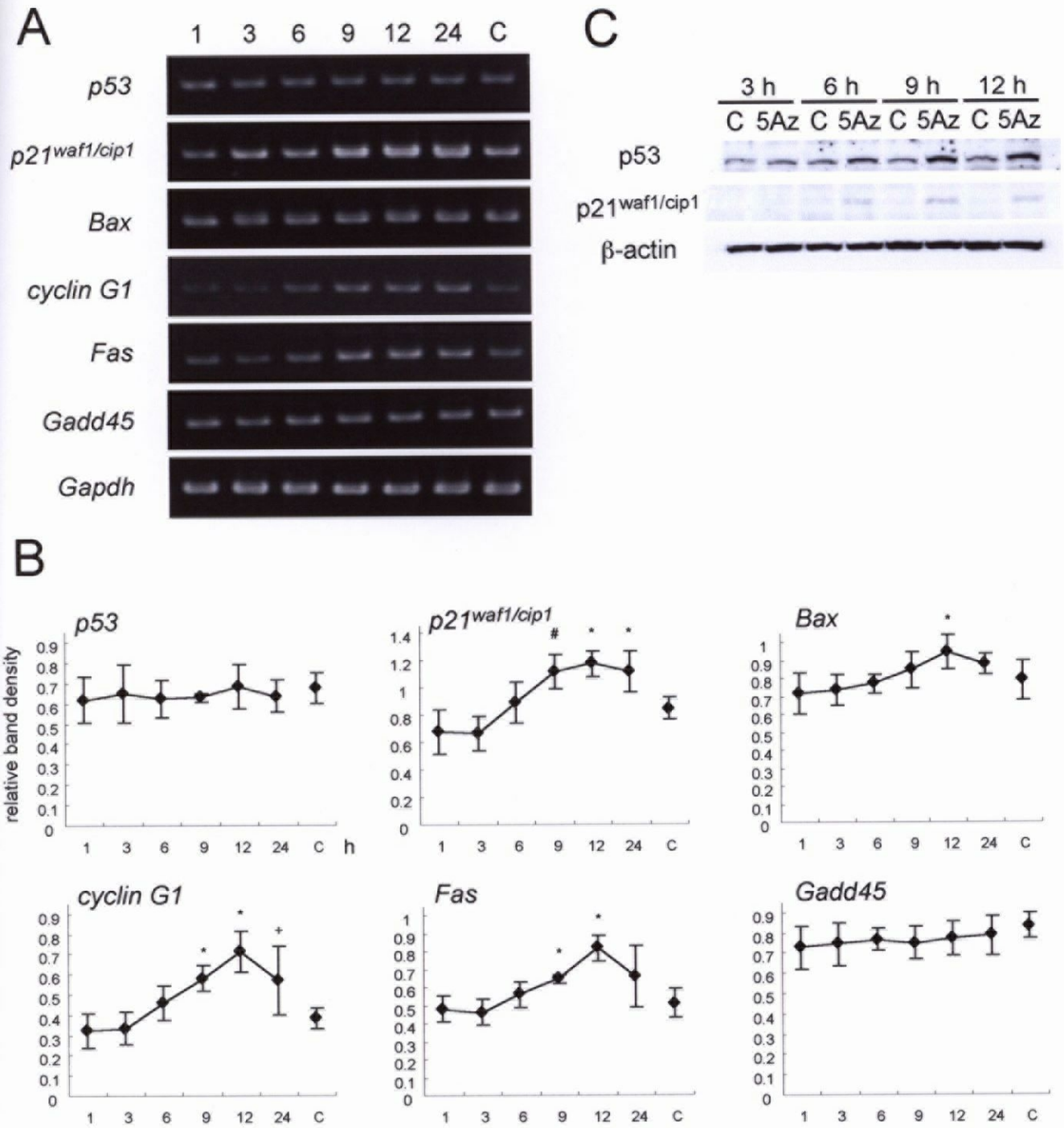

Fig. 2-2. Sequential changes in the expression of p53 and its transcriptional target genes. A: mRNA expression of *p53* and its transcriptional target genes (*p21*$^{waf1/cip1}$, *Bax*, *Fas*, *cyclin G1*, and *Gadd45*) from 1 to 24 h after 5AzC treatment and control (C) at 12 h. *Gapdh* was included as an internal control. B: Relative band density of mRNA expression. Each value represents the mean ± SD of 5 samples. Significant difference is shown by Student's *t*-test (*: $p<0.05$), Mann-Whitney's U test (#: $p<0.05$), and Weltch's *t*-test (+: $p<0.05$). Expression of *p21*$^{waf1/cip1}$, *Bax*, *cyclin G1*, and *Fas* were elevated. C: Western blot analysis of p53 and p21$^{waf1/cip1}$ in control (C) and 5AzC-treated (5Az) rat fetal telencephalon. The expression of p53 and its target gene, p21$^{waf1/cip1}$, increased from 6 to 12 h.

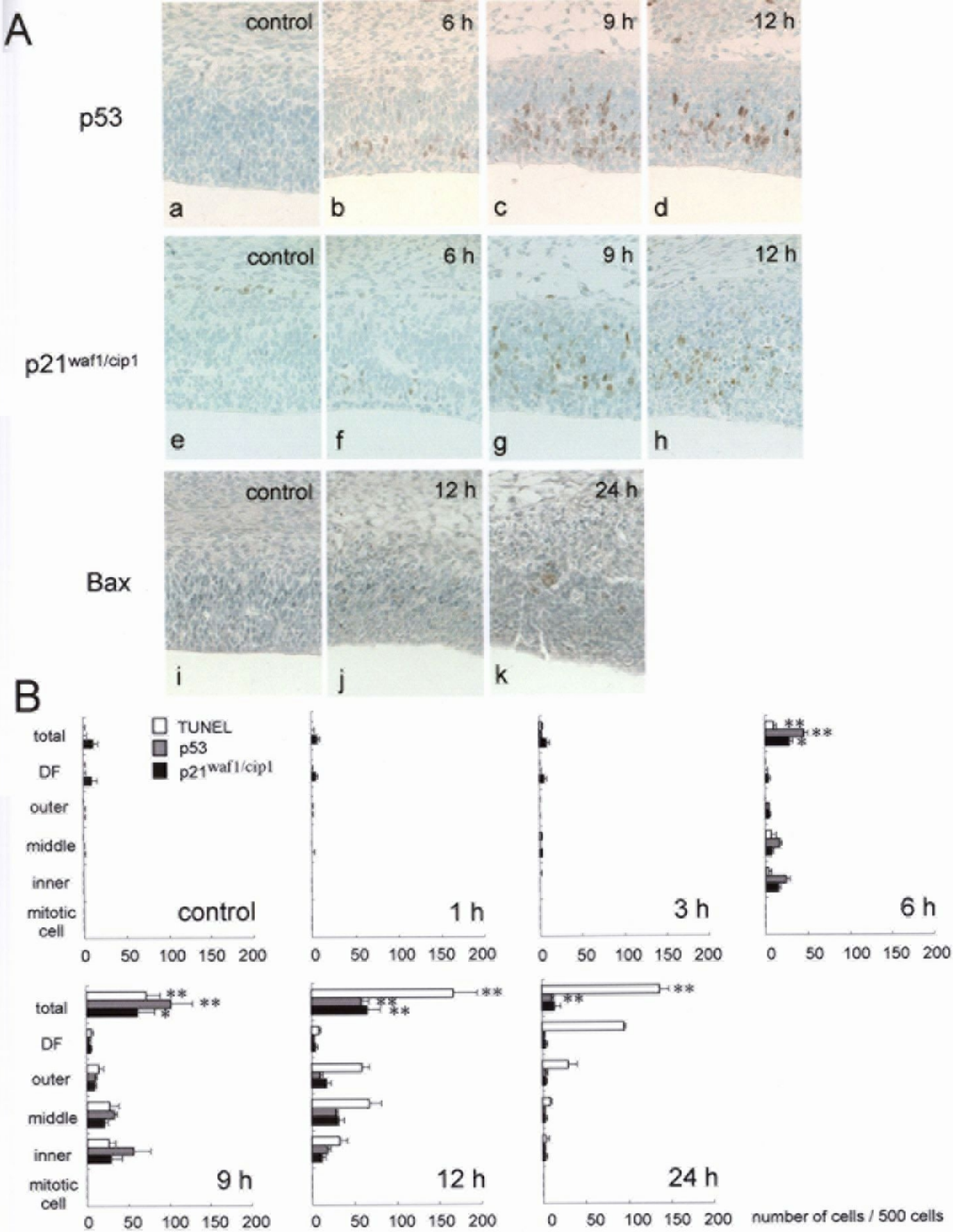

Fig. 2-3. Expression of p53, $p21^{waf1/cip1}$,and Bax protein, and its distribution in the telencephalic wall. A: p53 (a-d), $p21^{waf1/cip1}$ (e-h), and Bax (i-k) were detected immunohistochemically. a, e, i: control (12 h); b, f: 6 h; c, g: 9 h; d, h, j: 12 h; k: 24 h. B: The number of TUNEL (white bar), p53- (gray bar), and $p21^{waf1/cip1}$-positive cells (black bar) / 500 cells were counted in the 5 areas of the telencephalic wall (DF, outer, middle, inner, mitotic cell; Fig. I-2) . Each value represents the mean ± SD of 3 dams. Statistical analysis was done on the total numbers. *:$p<0.05$, **$p<0.01$; significantly different from the control group (Student's *t*-test).

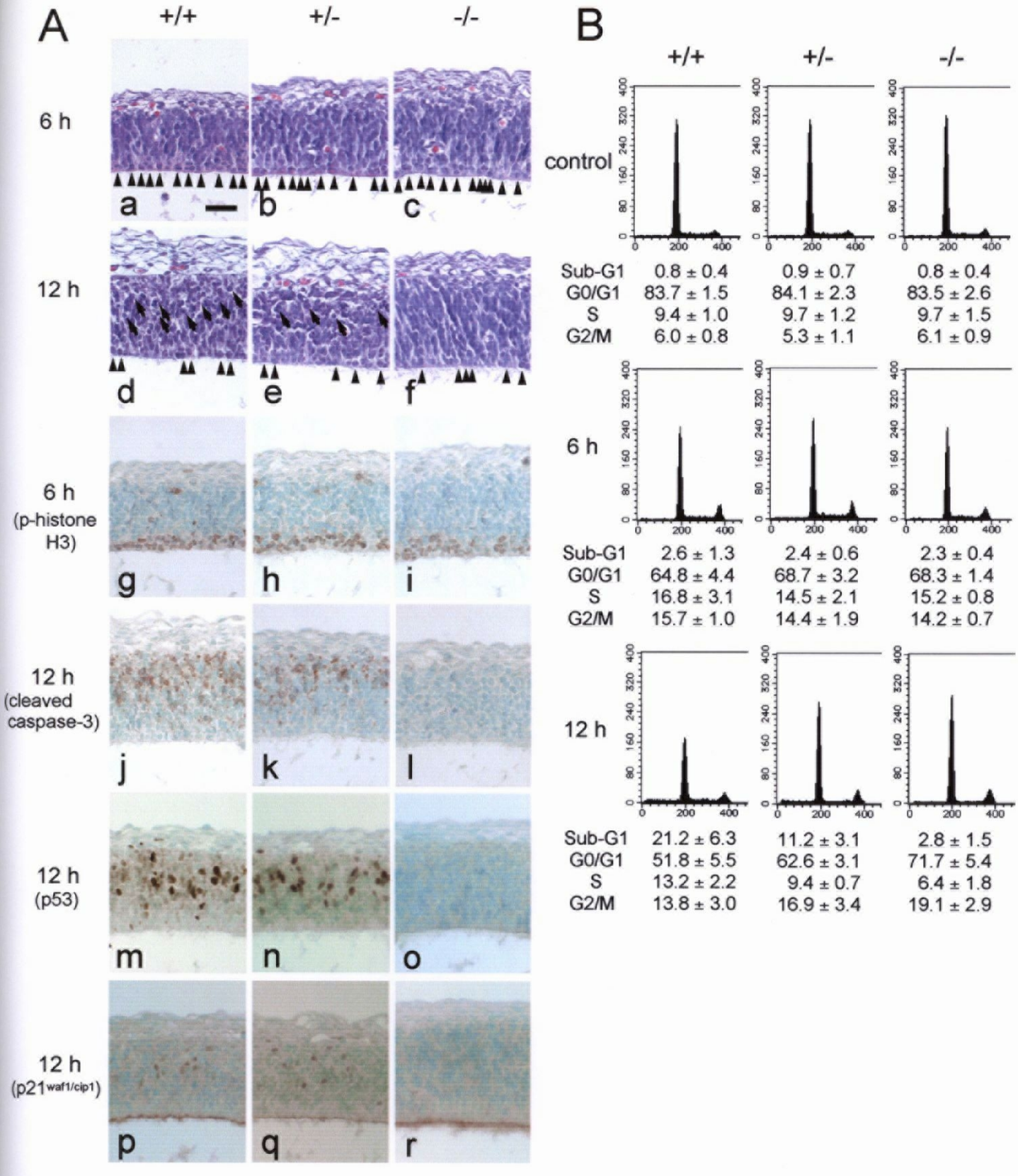

Fig. 2-4. 5AzC-induced p53-dependent apoptosis and p53-independent G2/M arrest. A: Histopathological changes in the VZ of dorsal telencephalic wall of p53-knockout mice fetus. (a-f): HE staining. (g-i): Phospho-histone H3 at 6 h. (j-l): Cleaved caspase-3 at 12 h. (m-o): p53 staining at 12 h. (p-r): $p21^{waf1/cip1}$ staining at 12 h. Accumulation of mitotic cells is observed in every p53 genotype (a-c and g-i, arrowheads: mitotic cells) and then decreased at 12 h (d-f, arrowheads: mitotic cells). Apoptosis is induced in $p53^{+/+}$ and $p53^{+/-}$ mice, but not in $p53^{-/-}$ mice (d-f and j-l, arrows: apoptotic cells). p53 and $p21^{waf1/cip1}$ are expressed in $p53^{+/+}$ and $p53^{+/-}$ mice, but not in $p53^{-/-}$ mice (m-o and p-r). Scale bar: 50 μm. B: Cell cycle analysis of telencephalic cells of p53-knockout mice fetuses (X axis: PI intensity (DNA content), Y axis: cell number). Percentages for each cell cycle phase are presented as the mean ± SD of 3 dams. In $p53^{+/+}$ and $p53^{+/-}$ mice, the number of G2/M phase cells increased at 6 h, and apoptosis in the sub-G1 area at 12 h. In $p53^{-/-}$ mice, the number of G2/M phase cells increased from 6 to 12 h, but apoptosis did not occur remarkably.

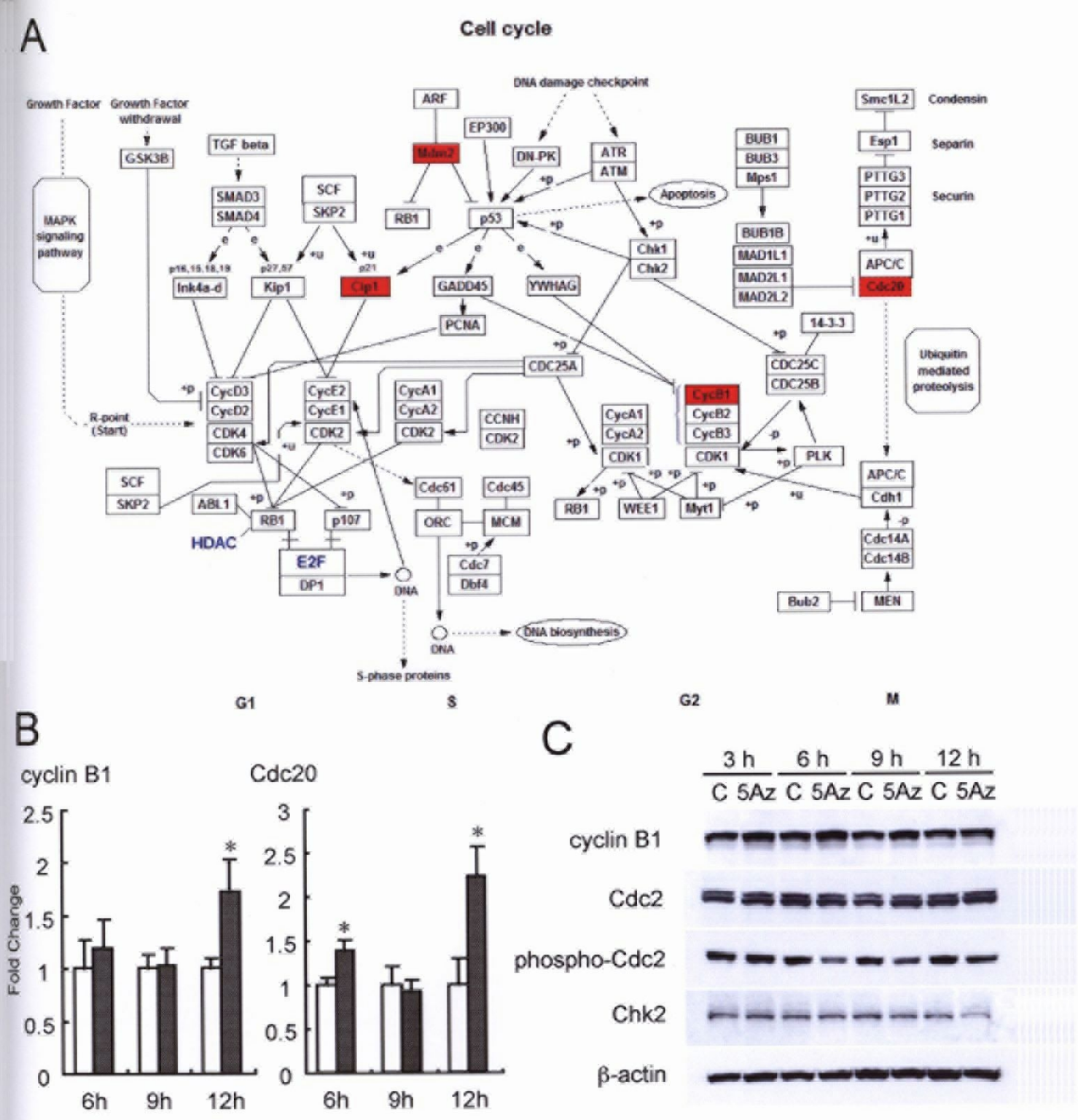

Fig. 2-5. Changes in the expression of G2/M phase regulators in 5AzC-treated rat fetal telencephalon. A: The cascade of cell cycle regulation showed by GenMAPP. Red labeled genes are the upregulated genes by 5AzC-treatment. They are p53-related genes (*p21*$^{waf1/cip1}$ and *Mdm2*) and G2/M regulating genes (*cyclin B1* and *Cdc20*). On the other hand, there are no downregulated genes. e, expression; +p, phosphorylation; -p, dephosphorylation; +u, ubiquitination. B: mRNA expression of G2/M regulating genes, *cyclin B1* and *Cdc20*, were examined by real-time PCR. The expression of both genes was upregulated at 12 h. *: $p < 0.05$; significantly different from the control group (Student's *t*-test). C: Western blot analysis of G2/M phase regulators of control (C) and 5AzC-treated (5Az) rat fetal telencephalon. The expression of cyclin B1 increased slightly from 3 to 9 h, and that of phosphorylated-Cdc2 (Tyr16) decreased from 6 to 12 h, suggesting the abnormal activation of G2 to M transition. The expression and mobility of Chk2 did not change through the experimental period.

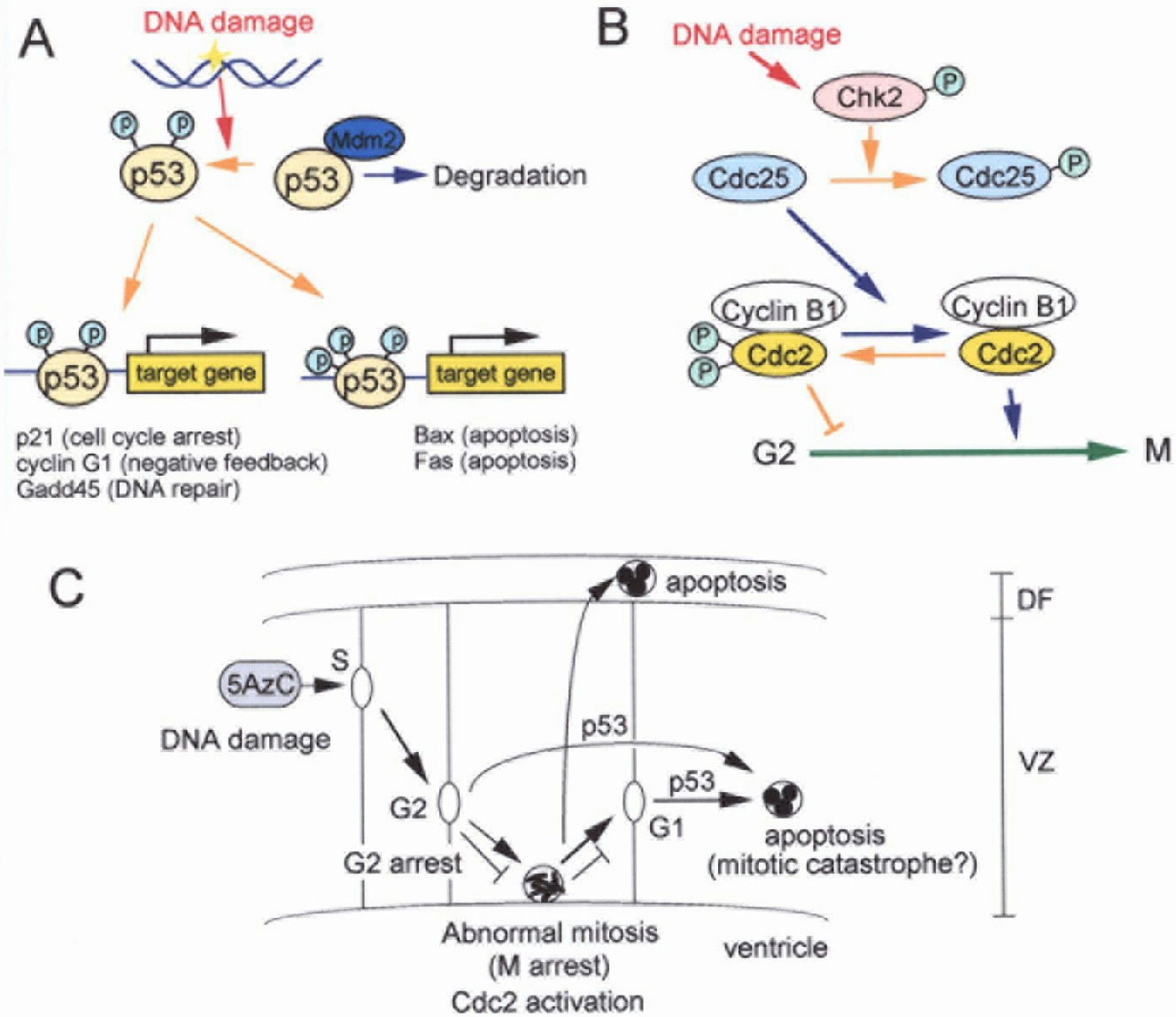

Fig. 2-6. Molecular mechanism of 5AzC-induced toxicity in the developing fetal brain. A: p53 is a transcription factor that regulates cell proliferation and cell death in response to DNA damage. DNA damage activates p53 via phosphorylation, which inhibits Mdm2-mediated p53 degradation. Phosphorylated p53 activates transcription of various target genes that play roles in cell cycle arrest and apoptosis. B: G2/M checkpoint. Normal cell cycle transition from G2 to M is dependent on Cdc2-Cyclin B1 complex , which is activated by Cdc25 (blue arrows). DNA damge activates Chk2 and inhibits Cdc25 function by phosphorylation (orange arrows). Absense of Cdc25 function leads to inactivation of Cdc2-Cyclin B1 complex by Cdc2 phosphorylation, which stops G2/M progression (orange arrow and line). C: The schema of the molecular mechanisms of 5AzC-induced cell cycle alteration and apoptosis. 5AzC would be incorporated into DNA in S phase and cause DNA damage. Damaged neural progenitor cells enter M phase with abnormal regulation, such as excess Cdc2 activation, and they are induced M arrest with abnormal morphologies along the ventricle. G2 arrest also occurs with delay in inward-migration. Then, the cells are divided into daughter cells, but undergo apoptosis in G1 phase. G2 phase cells also die by apoptosis. Apoptosis is induced in a p53-dependent mechanism, whereas the G2/M phase arrest is regulated in a p53-independent way.